

Nonspecific aggregation in native electrokinetic nanoelectrospray ionization



Kimberly L. Davidson^a, Derek R. Oberreit^{b,c}, Christopher J. Hogan Jr.^b, Matthew F. Bush^{a,*}

^a University of Washington, Department of Chemistry, Box 351700, Seattle, WA 98195-1700, United States

^b Department of Mechanical Engineering, University of Minnesota, Minneapolis, MN 55455, United States

^c Kanomax FMT, 4104 Hoffman Road, White Bear Lake, MN 55110, United States

ARTICLE INFO

Article history:

Received 14 April 2016

Received in revised form 23 July 2016

Accepted 22 September 2016

Available online 23 September 2016

Keywords:

Electrospray

Protein complexes

Noncovalent interactions

Charge reduction

Nonspecific interactions

ABSTRACT

Native mass spectrometry is widely used to determine the stoichiometries and binding constants of non-covalent interactions in solution. One challenge is that multiple analytes in a single electrospray droplet can aggregate during solvent evaporation, which will bias the distribution of oligomeric states observed during gas-phase measurements. Here, measurements of solution flow rates, electrospray currents, droplet size distributions, and nonspecific aggregation are used in conjunction with Poisson statistics to characterize the factors that control nonspecific aggregation during typical native mass spectrometry experiments. Using electrokinetic nanoelectrospray ionization and a 30 nA current, low flow rates of less than 10 nL min⁻¹ and initial droplets with mean diameters of ~60 nm were observed. For solutions containing 4 μM analyte under these conditions, Poisson statistics and charge-reduction drift tube ion mobility spectrometry both indicate that ~90% of the desolvated, occupied droplets contain a single analyte. Initial droplet sizes and contributions from nonspecific aggregates both increase with increasing current. Ion mobility mass spectrometry analysis of the ions produced using these conditions without charge reduction exhibit even less nonspecific aggregation (~2%). All approaches indicate that increasing the ionization current increases the flow rate, droplet size distribution, and extent of nonspecific aggregation. These results provide detailed insights into the role of small initial droplets in the success of native mass spectrometry.

© 2016 Elsevier B.V. All rights reserved.

1. Introduction

In native mass spectrometry, intact protein and protein complexes are formed using electrospray ionization (ESI) from aqueous buffered solutions that have a biologically relevant pH and ionic strength. Native mass spectrometry is now widely used to characterize the stoichiometry [1–7] and binding constants [8–10] of proteins, ligands, and metal ions in noncovalent complexes. For example, native mass spectrometry has been used to characterize intermediates in the assembly of disease-associated protein aggregates [1,3,7] and viral capsids [2,6,11]. Most studies implicitly or explicitly assume that the oligomeric distribution of the ions analyzed in these experiments resemble those of the corresponding noncovalent complexes in solution. However, if multiple analytes in a single droplet aggregate during the evaporation of the solvent,

the distribution of oligomeric states observed in the gas-phase measurements will be biased by the presence of nonspecific aggregates [12–14].

The charged-residue model is most-often used to explain the formation of multiply charged macromolecular ions. In this model, neutral solvent molecules evaporate from the initial charged droplet until the Coulombic repulsion exceeds the surface tension of the droplet (the Rayleigh limit) [15–17]. At this limit, Coulomb fission will result in the ejection of a progeny droplet with a smaller radius and a fraction of the charges of the precursor droplet [15]. This process repeats until complete desolvation results in the formation of a multiply charged, gas-phase analyte ion. During solvent evaporation, the concentration of solutes will increase, which may result in the formation of nonspecific aggregates when multiple solutes are present in a single droplet. The extent of nonspecific aggregates is therefore linked to both the original droplet size distribution and the size distributions of progeny droplets formed during fission events.

* Corresponding author.

E-mail address: mattbush@uw.edu (M.F. Bush).

Most fundamental studies of the ESI have used externally controlled solution flows through capillaries with inner diameters of tens to hundreds of micrometers [11,18–20], which will be referred to as constant-flow ESI. In contrast, most native mass spectrometry experiments use comparatively smaller inner diameter capillaries without an externally applied pressure. The flow rates in these experiments depend on the electroosmotic flow [21] of the solution that is induced by the applied electric field, which we refer to here as electrokinetic nanoESI. This implementation exhibits many advantages including reduced sample consumption [22], adduction of small molecules and ions [22,23], and nonspecific aggregation of analytes [23]. For example, electrokinetic nanoESI of the *E. Coli* chaperone GroEL yields well-resolved mass spectral peaks corresponding to different charge states of the biologically relevant tetradecamer [23]. Constant-flow ESI of the same sample using the same mass analyzer yields significantly broader peaks and relatively intense features corresponding to nonspecific dimers and trimers of tetradecamers [23].

Many strategies have been used to characterize the extent of nonspecific aggregation during ESI [24–27]. Klassen and coworkers pioneered the use of the “reporter molecule method” for protein-protein [25] and protein-ligand [26] complexes, in which measurements of the extent of aggregation during ESI for species that do not interact in solution are used to quantify the contribution of nonspecific aggregation to observed gas-phase oligomer distributions. The reporter molecule method reduces the bias of nonspecific interactions to measurements of binding affinities in solution. However, from those measurements alone, it is challenging to determine the contributions from different aspects of the ESI process, e.g., initial droplet sizes versus droplet fission, to nonspecific aggregation. Statistical approaches have also been used to relate the extent of aggregation during ESI to the bulk concentration of the analyte and the number of copies of an analyte present in a droplet, using either a log-normal distribution of diameters [12,28,29] or discrete diameter [13,14,27] for the droplet. For example, Monte Carlo simulations suggest that the extent of nonspecific aggregation observed in native mass spectrometry of solutions containing different concentrations of a dimeric protein were consistent with the aggregation of analytes from a 24 ± 3 nm radius droplet of the initial solution [27]. Using that effective droplet size, Monte Carlo simulations agreed well with the observed extent of aggregation during ESI for selected protein complexes that do not form higher-order complexes in solution [27].

The objective of this study is to use Poisson statistics and measurements of droplet size distributions, flow rates, and the extent of protein aggregation during electrokinetic nanoESI as a function of the ionization current to elucidate the factors that mitigate nonspecific aggregation in electrokinetic nanoESI. Low flow rates (less than 10 nL min^{-1}) and small initial droplet diameters ~ 60 nm are observed at ionization currents near the threshold of ion formation (30 nA). Both the flow rate and initial droplet diameters increased monotonically with ionization current; at 400 nA we observed evidence for initial droplets that had diameters of ~ 500 nm, which are comparable to those produced from constant-flow ESI sources [16,17,30]. Based on measured droplet sizes, probability calculations show the extent of nonspecific aggregation depends on ionization current and analyte concentration. For example, the majority of the occupied droplets that are less than 100 nm from solutions with $4 \mu\text{M}$ analyte contain a single analyte. In contrast, the majority of occupied droplets that are greater than 100 nm from solutions with $4 \mu\text{M}$ analyte contain multiple analytes, which could lead to nonspecific aggregation during desolvation. The predictions from these calculations are generally consistent with our measurements of nonspecific aggregation observed from ion mobility spectrometry of charge-reduced droplets containing myoglobin and standard native ion mobility mass spectrometry experiments.

These results provide insights into the advantages of small initial droplet diameters for obtaining accurate oligomeric distributions of protein complexes in native mass spectrometry experiments.

2. Experimental methods

2.1. Electrokinetic NanoESI

The ion source used for these experiments consists of a platinum wire electrode inserted into a borosilicate capillary emitter filled with $\sim 3 \mu\text{L}$ of solution. The capillary has an inner diameter of 0.78 mm that was pulled to a tip with an inner diameter of 1 to $3 \mu\text{m}$ using a micropipette puller (Sutter Instruments Model P-97; Novato, CA). A Bertan Power Supply (Model 205B-10R or 205B-03R; Hauppauge, NY) controlled the potential of the platinum wire, which was in direct contact with the solution. Ionization currents were measured using a digital multimeter (Jameco Benchpro DT 830B; Belmont, CA) that was positioned between the power supply and the platinum wire electrode. In most experiments, the electro-spray potential was adjusted to maintain constant current.

2.2. Flow rate

Flow rates were determined using the difference in the weight of the capillary before and after spraying at a constant ionization current for a timed interval, then converting that difference to a volume using the density of aqueous 200 mM ammonium acetate (1.00 g cm^{-3}). The capillary and tip holder were weighed using an analytical balance (Mettler Toledo XS105; Columbus, OH). Errors were propagated from the manufacturer's specification for the accuracy of the balance (± 0.01 mg) and are consistent with technical replicates. Mass spectra were acquired simultaneously using a Waters Synapt G2 HDMS (Wilmslow, United Kingdom) to confirm ionization.

2.3. Apparent droplet size distributions

The distributions of droplet diameters produced by the electrokinetic nanoESI source were measured using charge reduction ion mobility analysis with a differential mobility analyzer [31–35]. An ESI capillary containing 0.1% by volume sucrose in aqueous 200 mM ammonium acetate was positioned less than 5 mm from a $10 \text{ mCi } ^{210}\text{Po}$ source (Nucleospot; Grand Island, NY). This source produces roughly equal concentrations of cations and anions from trace species in the air [36] surrounding the sampled droplets. Via droplet-ion collisions, droplets are charge reduced, which mitigates Coulomb fission. Droplets hence evaporate with minimal fissions, leaving non-volatile residue clusters whose sizes (diameters) are directly linked to the initial droplet size [37]. After exposure to the ^{210}Po generated ions, the residue clusters are additionally brought towards a known charge distribution [38] in which most have charges states of 0, -1 , or $+1$, but multiply charged residue clusters can remain if clusters do not achieve this steady charge distribution, a common occurrence for droplets generated by ESI. The resulting sucrose clusters were mobility-filtered using a differential mobility analyzer [39] (TSI Model 3085; Shoreview, MN) and detected using a condensation particle counter [40] (TSI Model 3786), which were operated as a scanning mobility particle sizer [41]. Using data inversion [42], the residue and droplet size distributions were inferred.

2.4. Drift tube ion mobility

In conjunction with charge reduction via ^{210}Po generated ions, ion mobility measurements were also made on electrokinetic nanoESI generated ions using a drift-tube ion-mobility spectrometer (DT-IMS) operated at atmospheric pressure with a counterflow

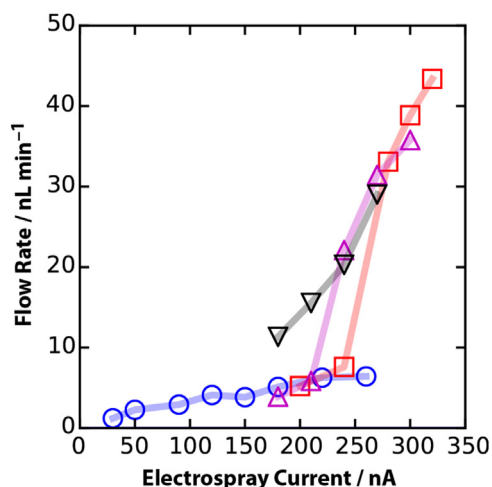


Fig. 1. Representative flow rates measured as a function of ESI current. When using a new capillary at each current (blue circles), flow rates remained less than 10 nL min^{-1} over a broad range of currents. When using a single capillary and monotonically increasing the current (red squares), the flow rates exhibited a sharp increase in flow rate at currents greater than 200 nA . The results shown using magenta triangles are from a replicate of the preceding experiment and exhibited similar trends. Immediately after acquiring those results and using the same capillary, flow rates were measured using monotonically decreasing currents (black triangles). The latter flow rates are greater than those measured using monotonically increasing currents, suggesting that the capillary was compromised while using high currents. The uncertainties in flow rate are comparable to size of markers plotted.

of gas [43]. The drift region of the DT-IMS employed is 224 mm long and consists of 20 stainless steel ring electrodes that have a 40 mm inner diameter, 10 mm width, and are separated by 2 mm wide insulators. A 9 kV DC potential was applied to the first ring electrode; the potential decreases nearly linearly across the drift tube [43] and establishes a uniform axial electric field. After charge reduction (again using a ^{210}Po source) and subsequent desolvation, the ions entered the drift region and were separated based on their mobilities and quantified by their arrival times at a condensation particle counter placed downstream of the DT-IMS.

3. Results and discussion

3.1. Native electrokinetic NanoESI

Most ESI droplet size studies have used externally controlled flow rates and large inner diameter capillaries (10 s – 100 s μm , constant-flow ESI). These studies have shown that droplet sizes depend on the applied voltage (and therefore ionization current) [44], flow rate [45], and capillary orifice diameter [46]. In contrast, few studies have focused on the droplet sizes generated from nanoESI using electrokinetic controlled solution flow through smaller inner diameter capillaries (less than 5 s μm), *i.e.*, the conditions used most frequently for native mass spectrometry. To investigate the effects of applied voltage, and therefore current, on the flow rates in electrokinetic nanoESI, a solution containing 4 s μM myoglobin from horse heart (selected arbitrarily) in 200 mM ammonium acetate at $\text{pH} = 7.0$ was electrosprayed using a range of currents and typical conditions for native mass spectrometry. Flow rates of 1.2 – 6.4 nL min^{-1} were measured using currents from 30 to 260 nA (Fig. 1) and a different tip for each measurement. For comparison, currents of less than 100 nA are used for most applications of native mass spectrometry performed in our lab. When the same tip was used for each measurement, a sudden increase in the flow rate, to greater than 20 nL min^{-1} , was often observed using higher ionization currents (between 220 and 280 nA). After this sudden increase, subsequent flow rates measured using lower cur-

rents were greater than those measured originally. The irreversible change in flow rate is attributed to physical deformation of the capillary tip.

The flow rates measured here are slower than those reported previously for similar electrokinetic nanoESI sources in which the potential was applied to a thin gold coating on the outside of the capillary. For example, using gold-coated capillaries and ionization currents of 10 , 16 , and 10 to 145 nA , flow rates of 20 [18], 20 [47], and 9 – 589 [19] nL min^{-1} , respectively, have been reported. Those studies used different capillaries and solvents other than the 200 mM ammonium acetate used in this work, which may account for the differences in flow rate (e.g. different surface tensions). In contrast, constant-flow ESI sources generally use flow rates in the $\mu\text{L min}^{-1}$ range [18,20].

3.2. Initial droplet size distributions

To investigate the effects of flow rate from the electrokinetic nanoESI source on droplet size, charge reduction ion mobility measurements [31–35] of sucrose residue clusters were used to infer droplet size distributions. The residue measurement approach (as described in the Experimental methods) has been used previously to characterize droplet size distributions from ESI and is considered a reliable, albeit indirect, means to estimate original ESI droplet size [37]. Fig. 2A shows the distribution of apparent initial droplet diameters as a function of electropray potential; the corresponding currents are also shown. Fig. 3A shows the distribution of initial droplet diameters determined using an ionization current of 30 nA , which is near the threshold for ionization. This distribution has a mean diameter of $\sim 60 \text{ nm}$. However, we consider this to be an upper limit for the mean; the condensation particle counter employed has a lower detection limit near 4.5 nm [40], hence residue clusters corresponding to droplets smaller than 45 nm in diameter (4.5 nm and below) were not detected efficiently.

In most native mass spectrometry experiments, electrokinetic nanoESI sources are operated near the threshold for ionization. Our results indicate that this results in the formation of very small initial droplets. These droplet sizes are considerably smaller than those reported previously using constant-flow ESI sources (even those qualified as “nano-ESI” sources). Using similar implementations of the residue measurement approach and constant-flow ESI sources, Chen et al. reported 280 nm droplets using a current of 300 nA [37] and Hogan et al. reported 170.56 nm diameter droplets using currents of 200 – 300 nA [11]. Light scattering has also been used to characterize the droplets produced by constant-flow ESI sources, but typically for droplets that are significantly larger than those in the present study (e.g., $\sim 25 \text{ s}$ μm) [17].

Increasing the ionization current results in the formation of larger droplets (Fig. 2A, subpopulation III). Interestingly, additional features are also present at currents greater than 50 nA . For example, the distribution of apparent droplet diameters determined using an ionization current of 75 nA is shown in Fig. 4A and exhibits features for subpopulations with mean apparent diameters near 220 , 140 , and 75 nm . With increasing ionization current, features for three subpopulations (labeled I, II, and III, respectively) persist with monotonically increasing diameters.

We propose two possible assignments for subpopulations I and II. The first candidate assignment is that subpopulations I and II correspond to the progeny droplets resulting from Coulomb fission from subpopulations II and III, respectively. Though satellite features have been detected in prior examinations of ESI generated droplets (leading to bimodal distributions) [15,37,48], the appearance of such monomodal progeny distributions has not been reported in other studies using the residue measurement approach. This result would be consistent with droplet fission occurring faster than charge reduction. The rate of droplet evaporation (in terms

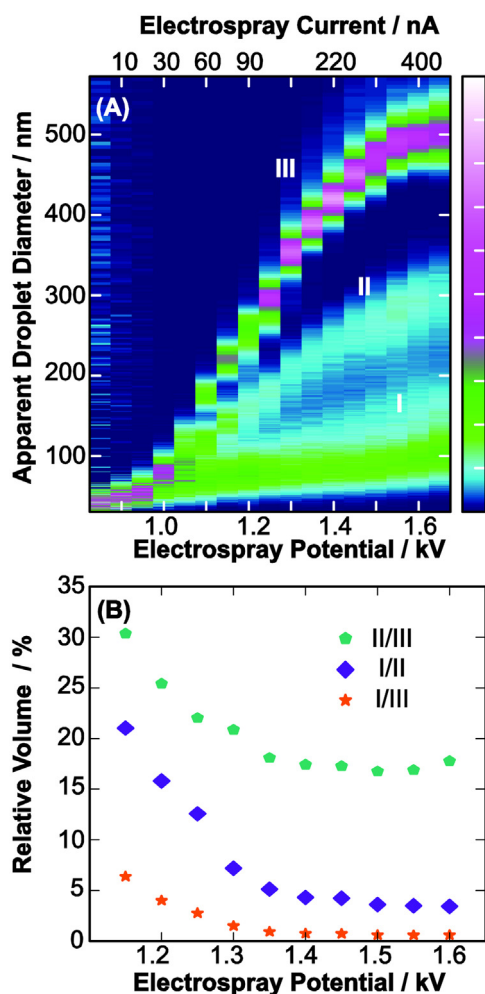


Fig. 2. (A) A heat map of apparent droplet diameters as a function of increasing potential/current. As the ionization current increases, the initial droplet diameters increase (subpopulation III) and additional features appear (subpopulations I and II). (B) The masses of the progeny droplets relative to the parent droplets based on the apparent diameters for subpopulation II from subpopulation III (turquoise pentagons), subpopulation I from subpopulation II (purple diamonds), and subpopulation I from subpopulation III (orange stars).

of diameter) increases with decreasing droplet size [49], therefore smaller droplets can more readily access the Rayleigh limit before they are fully charged reduced relative to larger droplets produced using constant-flow electro spray sources. For comparison, modelling of collisions between charged particles and a charged aerosol that is 200 nm in diameter suggests that charge reduction will occur on a millisecond timescale [50], whereas droplet fission from submicron droplets above the Rayleigh limit can occur on the microsecond time scale [48].

Fig. 2B shows that, using the first candidate assignment, the volumes of the droplets in subpopulation II are 20%–30% of those in subpopulation III. These values are similar to those reported in early measurements of mass loss during droplet fission of micron-scale droplets [51], but considerably greater than values reported based on more contemporary measurements (1%–5%) [17,52–54]. Although those studies [17,51–54] all probed droplets that were considerably larger (4–200 μm), the significant differences in mass loss strongly disfavor the assignment of subpopulation II as the progeny of subpopulation III. Furthermore, the formation of such large progeny droplets (20%–30% relative mass) would significantly broaden subpopulation III due to the loss of mass from the parent droplets.

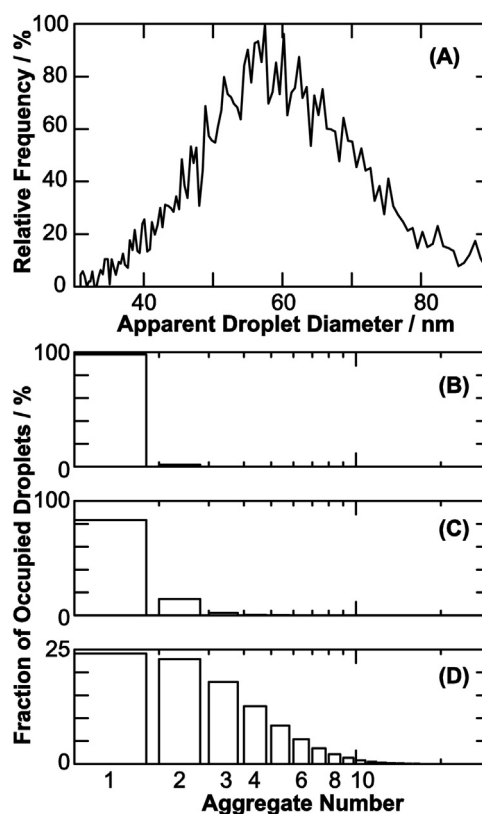


Fig. 3. (A) Droplet size distribution measured using an electro spray current of 30 nA. The total probability for each aggregate number was calculated using Eq. (3), the experimental droplet size distribution in (A), and analyte concentrations of 0.4 (B), 4 (C), and 40 (D) μM .

The second candidate assignment is that subpopulation II is composed of doubly charged analogues of subpopulation III, which would have greater mobility and appear to have smaller diameters in this analysis that assumes that all ions are singly charged. Subpopulation I is then assigned to the progeny droplets formed via Rayleigh fission of droplets that appear as subpopulations II and III. Fig. 2B shows that, using these assignments, the droplets in subpopulation I have comparable relative volumes to those reported previously [17,52–54]. Furthermore, the actual diameters of doubly charged forms of subpopulation II would be twice their apparent diameters, which would be similar to, albeit slightly larger than, the apparent diameters observed for subpopulation III. Therefore, these results are most consistent with the second candidate assignment and the presence of a non-negligible number of multiply charged residues remaining in the aerosol phase after exposure to the charge reduction source.

3.3. Theoretical nonspecific aggregate distributions

The frequency of nonspecific aggregates, assuming analyte concentrations of 0.4, 4.0, and 40 μM was predicted from the experimental droplet size distributions using the Poisson distribution. First, the mean aggregate size (number of monomers per aggregate), \bar{n} , is:

$$\bar{n}(D, C) = C \times \frac{4\pi}{3} \left(\frac{D}{2}\right)^3 \times N_A \quad (1)$$

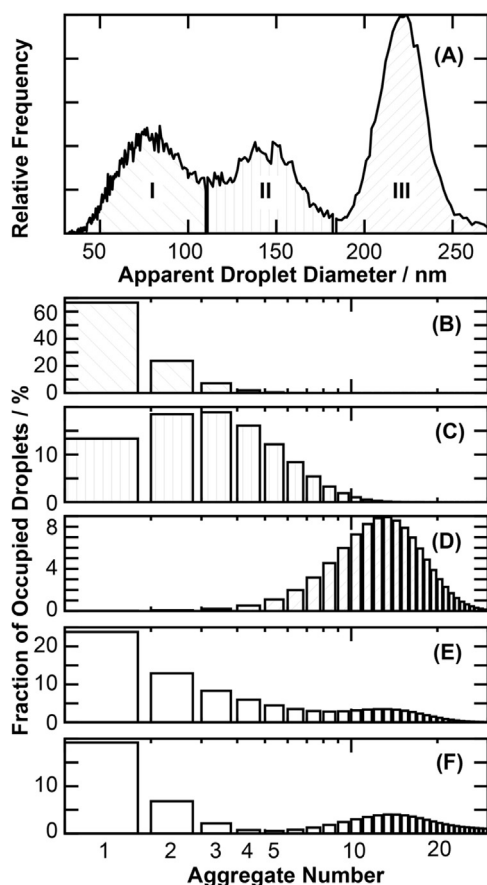


Fig. 4. (A) Droplet size distribution measured using an electrospray current of 75 nA, which includes contributions from subpopulations I, II, and III. The probability for each aggregate number was calculated using Eq. (3), an analyte concentration of 4 μM , and assuming that the distribution of apparent droplet diameter accurately reflects the actual distribution of droplet diameters. (B), (C), and (D) show results for subpopulations I, II, and III, respectively. (E) shows the probability for each aggregate number calculated for the entire distribution using the same assumption. (F) shows the probability for each aggregate number calculated assuming that subpopulation II is for doubly charged ions; thus the actual diameters are twice the apparent diameters. Analogous plots determined using concentrations of 0.4 and 40 μM are shown in Figs. S1 and S2, respectively.

where D is the droplet diameter, C is the analyte concentration, and N_A is Avogadro's number. Assuming Poisson statistics, the probability of each aggregate size, n , is:

$$P(n, D, C) = \frac{\bar{n}(D, C)^n e^{-\bar{n}(D, C)}}{n!} \quad (2)$$

Prior studies using Eq. (2) to examine ESI-induced aggregation used either a log-normal distribution [12,28,29] or a discrete diameter [13,14] for the droplet. Here, we consider the total aggregate distribution expected from these experiments, which depends on the experimental droplet size distribution $I(D)$ and Eq. (2):

$$P_{\text{total}}(n, C) = \sum_D [I(D)P(n, D, C)] \quad (3)$$

Note that this approach does not account for the volume of the analyte. This effect is expected to be negligible for small proteins and aggregate sizes, but it will be increasingly significant with increasing droplet occupancy and analyte size. Furthermore, this analysis does not consider any protein-specific effects that may affect nonspecific aggregation.

The total aggregate distribution expected for the apparent droplet size distribution shown in Fig. 3A was calculated using concentrations of 0.4, 4.0, and 40 μM and are shown in Figs. 3B, C, and D, respectively. This analysis suggests that the fraction of

occupied droplets containing a single analyte is 98%, 83%, and 24% for 0.4, 4, and 40 μM analyte concentrations, respectively. Thus when using the lowest concentrations and an ionization current of 30 nA, which is similar to that used in many structural biology applications, excellent fidelity between the aqueous and gas-phase oligomeric states will be achieved.

The distribution of apparent droplet diameters determined using an ionization current of 75 nA is shown in Fig. 4A and exhibits features for subpopulations with mean apparent diameters near 220, 140, and 75 nm (III, II, and I, respectively). The total aggregate distribution expected for each subpopulation assuming that the apparent droplet diameters accurately reflect the actual droplet diameters and a concentration of 4 μM are shown in Figs. 4B, C, and D, respectively. This analysis suggests that 67% of the occupied droplets within subpopulation I contain a single analyte, which will yield ions with the correct stoichiometry after desolvation, whereas 33% contain multiple analytes, which may yield nonspecific aggregates (Fig. 4B). Occupied droplets within subpopulation II are large enough to contain a wider range of aggregate sizes with a 19% probability of containing three analytes (trimer, Fig. 4C). Greater than 99% of droplets that are within subpopulation III contain multiple analytes (Fig. 4D). Therefore, oligomeric state distributions determined using droplets that are ~ 200 nm or larger will deviate radically from the corresponding solution-phase distributions.

The total aggregate distribution for the entire apparent droplet size distribution using a concentration of 4 μM is shown in Fig. 4E. This analysis suggests that 24% of the occupied droplets contain a single analyte, whereas 76% contain multiple analytes and may lead to nonspecific aggregates. As discussed earlier, it is likely that subpopulation II is attributable to doubly charged ions. In that case, the actual diameters of these droplets are likely twice that of the apparent diameters due to their increased mobilities. The actual volumes of those droplets are eight-fold greater than that suggested by their apparent diameters. Fig. 4F shows the total aggregate distribution expected using those assignments. This analysis suggests that only 19% of the droplets contain a single analyte, whereas 81% contain multiple analytes. Analogous distributions determined using the 75 nA droplet-size distribution and analyte concentrations of 0.4 and 40 μM are shown in Supporting information Figs. S1 and S2, respectively, which further illustrate the advantage of using lower analyte concentration to mitigate nonspecific aggregation.

3.4. Nonspecific aggregation during native charge-reduction ESI

The effects of current and concentration on nonspecific aggregation were measured experimentally using varying concentrations of myoglobin in aqueous 200 mM ammonium acetate solutions. Myoglobin is a 17.6 kDa protein that exists as a monomer in solution, thus, the presence of higher-order oligomers can be attributed to nonspecific aggregation. ESI droplets were charge reduced using ^{210}Po and the resulting ions were analyzed using an atmospheric pressure aspirating drift tube ion mobility spectrometer (DT-IMS) [43]. Separation in drift time depends on analyte size and shape, therefore, drift times increase with increasing oligomeric size.

The drift times measured using 4 μM myoglobin solutions and ionization currents ranging from 30 to 200 nA are shown in Fig. 5A. The intense feature centered near 2.50 s corresponds to monomeric myoglobin. Features at longer drift times correspond to higher-order oligomers of myoglobin. At the lowest stable current measured from the electrokinetic nanoESI source (30 nA), monomeric myoglobin was observed predominately (at least 90% relative abundance). This result is consistent with that from Poisson statistics that estimated 83% monomeric abundance for the apparent droplet size distribution measured at 30 nA. As the ionization current was increased, a feature corresponding to a relatively low abundance of nonspecific dimers appeared near 3.25 s. At 200 nA,

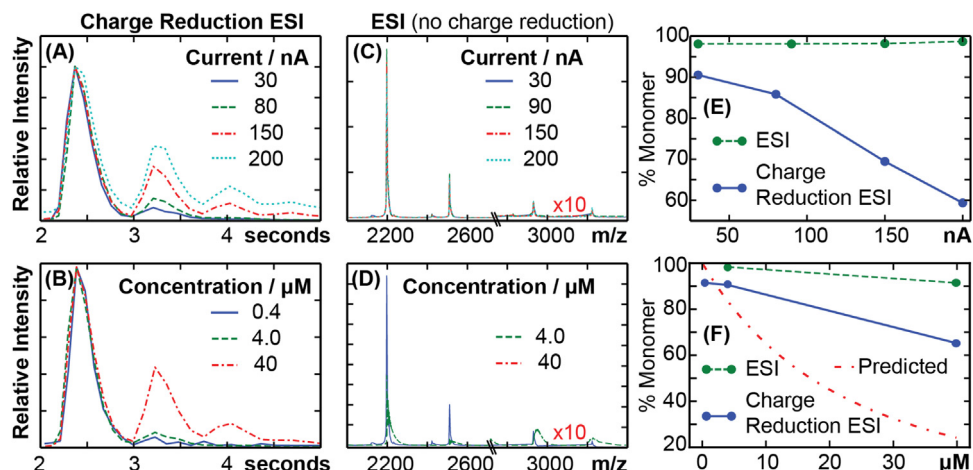


Fig. 5. (A) DT-IMS arrival-time distributions for 4.0 μM myoglobin in 200 mM ammonium acetate measured using currents of 30, 80, 150, and 200 nA with charge reduction. Increasing current increases the abundance of higher-order aggregates. (B) DT-IMS arrival-time distributions for 0.4, 4.0, and 40 μM myoglobin measured using a current of 30 nA with charge reduction. Nonspecific dimers increase greatly in intensity with increasing concentration. (C) Mass spectra for 4.0 μM myoglobin measured using currents of 30, 90, 150, and 200 nA. (D) Mass spectra of 4.0, and 40 μM myoglobin measured using a current of 30 nA. (E) Summarizes the results in (A) and (C). (F) Summarizes the results in (B), (D), and that obtained using the apparent droplet size distribution shown in Fig. 3A and Poisson statistics.

features that are assigned to trimers (4.00 s) and tetramers (4.75 s) also appeared. These results are generally consistent with the analysis based on apparent droplet size measurements and the Poisson distribution, which indicate a significant increase in the extent of nonspecific aggregation with increasing ionization current and the concomitant increase in droplet sizes.

To test the dependence of nonspecific aggregation on concentration, increasing concentrations of myoglobin (0.4, 4.0, and 40 μM) in 200 mM ammonium acetate (Fig. 5B) were analyzed using DT-IMS. A 30 nA current was used to minimize the formation of larger droplets. Consistent with the analysis above, increasing concentrations of myoglobin result in the formation of higher-order nonspecific aggregates due to increased droplet occupancy.

The percent of detected myoglobin monomer was calculated as functions of current (Fig. 5E) and concentration (Fig. 5F). When droplets were charge-reduced, there was a significant decrease in the relative abundance of monomer, from 91% to 59%, with increasing current. Therefore, there was a concomitant increase in nonspecific aggregate formation with increasing current. This trend also occurred with increasing concentration of myoglobin at a constant ionization current of 30 nA; the presence of monomer decreased from 91% to 65% with increasing concentration. These results are greater than the predicted percent monomer as a function of concentration determined using the apparent droplet size distribution in Fig. 3A and Poisson distribution (Fig. 5F), which decreases from 99% to 24% over the same range of concentrations. These differences suggest that the DT-IMS instrument may have a detection bias or that not all proteins in a single, charge-reduced droplet go on to form nonspecific aggregates.

3.5. Nonspecific aggregation during native ESI

The preceding experiments all used charge-reduction ESI, in which ESI is performed in the presence of ^{210}Po that reduces the number of charges on the droplets and inhibits Rayleigh fission [37]. In contrast, most native mass spectrometry experiments do not use charge reduction during ESI and the resulting droplets are more likely to exceed the Rayleigh limit and undergo Coulomb fission. In order to investigate these effects, nonspecific aggregation of myoglobin was characterized as a function of analyte concentration and ionization current using native electrokinetic nanoESI.

Ion mobility mass spectra from solutions containing 4.0 and 40 μM myoglobin were measured using a range of ionization cur-

rents (mass spectra shown in Fig. 5C). The spectrum of 4.0 μM myoglobin ions at an ionization current of 30 nA was additionally compared to a spectrum of 40 μM myoglobin ions at the same ionization current (Fig. 5D). With an increase in concentration, there was a shift to higher m/z due to adduction of small ions. The arrival time distributions confirmed that the peaks for the monomers and dimers appear at unique m/z values in these experiments.

For multiply charged droplets, the relative abundance of nonspecific aggregates ($\sim 2\%$) depended weakly on current and concentration over the ranges investigated. This result is consistent with the increased formation of smaller droplets resulting from fission events (Figs. 5E and F). Furthermore, this result suggests that monomeric ions resulting from these smaller droplets are detected with greater efficiency in the IM-MS experiments than the corresponding ions of aggregates from larger droplets. This result is in contrast to experiments using charge-reduced droplets that preserved monomeric oligomers at low currents (less than 50 nA) and concentrations (0.4 μM), but produced increasing abundances of higher-order aggregates with both increasing current and concentration. However, the relative abundance of monomers in the DT-IMS experiments is still less than expected based on the analysis of droplet size distributions measured using the same charge-reduction ESI source.

4. Conclusions

Over the last two decades, native mass spectrometry has established itself as a powerful tool for determining the stoichiometry and binding constants of noncovalent interactions in solution. This approach leverages the fidelity between the distributions of noncovalent complexes in solution and in the gas phase, although any nonspecific aggregation that occurs during the ionization process will bias these results. In this work, we evaluated the factors that contribute to nonspecific aggregation in native electrokinetic nanoESI using measurements of flow rate, current, droplet size distributions, and nonspecific aggregation in conjunction with Poisson statistics. These results show that using a typical ionization current (30 nA) and concentration (4 μM) for native mass spectrometry, electrokinetic nanoESI yields low flow rates (less than 10 nL min^{-1}) and small initial droplets ($\sim 60 \text{ nm}$ diameters) that predominately contain up to 1 analyte. Increasing the ionization current results in the formation of larger initial droplets that are more likely to contain multiple analytes, which may aggregate during solvent

evaporation and result in the formation of nonspecific aggregates that would bias the gas-phase measurement.

Most of the experiments reported here used charge reduction during ionization, which reduces the number of Coulomb fission events that occur during desolvation. The formation of progeny droplets decreases the fraction of occupied droplets that contain multiple analytes, consistent with decreased nonspecific aggregation observed in experiments without charge reduction relative to experiments with charge reduction. The combination of very small initial droplet sizes (~60 nm) and increased droplet fission in electrokinetic nanoESI without charge reduction has enabled the success of native mass spectrometry in quantifying the stoichiometries and affinities of noncovalent interactions in solution, even at μM concentrations.

Acknowledgements

M.F.B. and K.L.D. acknowledge support from the University of Washington. Support from US National Science Foundation Grant CBET-1133285 was used to the purchase of consumables for operation of the charge reduction ESI experiments. D.R.O. acknowledges support from a National Science Foundation Graduate Research Fellowship.

Appendix A. Supplementary data

Supplementary data associated with this article can be found, in the online version, at <http://dx.doi.org/10.1016/j.ijms.2016.09.013>.

References

- [1] U.I. Ekeowa, J. Freee, E. Miranda, B. Gooptu, M.F. Bush, J. Perez, et al., Defining the mechanism of polymerization in the serpinopathies, *Proc. Natl. Acad. Sci. U. S. A.* 107 (2010) 17146–17151, <http://dx.doi.org/10.1073/pnas.1004785107>.
- [2] C. Uetrecht, I.M. Barbu, G.K. Shoemaker, E. van Duijn, A.J.R. Heck, Interrogating viral capsid assembly with ion mobility–mass spectrometry, *Nat. Chem.* 3 (2011) 126–132, <http://dx.doi.org/10.1038/nchem.947>.
- [3] C. Bleiholder, N.F. Dupuis, T. Wyttenbach, M.T. Bowers, Ion mobility–mass spectrometry reveals a conformational conversion from random assembly to β -sheet in amyloid fibril formation, *Nat. Chem.* 3 (2011) 172–177, <http://dx.doi.org/10.1038/nchem.945>.
- [4] M. Zhou, N. Morgner, N.P. Barrera, A. Politis, S.C. Isaacson, D. Matak-Vinkovic, et al., Mass spectrometry of intact V-type ATPases reveals bound lipids and the effects of nucleotide binding, *Science* 334 (2011) 380–385, <http://dx.doi.org/10.1126/science.1210148>.
- [5] G.R. Hilton, J.L.P. Benesch, Two decades of studying non-covalent biomolecular assemblies by means of electrospray ionization mass spectrometry, *J. R. Soc. Interface* 9 (2012) 801–816, <http://dx.doi.org/10.1098/rsif.2011.0823>.
- [6] E.E. Pierson, D.Z. Keifer, L. Selzer, L.S. Lee, N.C. Contino, J.C.-Y. Wang, et al., Detection of late intermediates in virus capsid assembly by charge detection mass spectrometry, *J. Am. Chem. Soc.* 136 (2014) 3536–3541, <http://dx.doi.org/10.1021/ja411460w>.
- [7] A.C. Leney, C.L. Pashley, C.A. Scarff, S.E. Radford, A.E. Ashcroft, Insights into the role of the beta-2 microglobulin D-strand in amyloid propensity revealed by mass spectrometry, *Mol. Biosyst.* 10 (2014) 412–420, <http://dx.doi.org/10.1039/C3MB70420C>.
- [8] S.A. Hofstadler, K.A. Sannes-Lowery, Applications of ESI–MS in drug discovery: interrogation of noncovalent complexes, *Nat. Rev. Drug Discov.* 5 (2006) 585–595, <http://dx.doi.org/10.1038/nrd2083>.
- [9] E.N. Kitova, A. El-Hawiet, P.D. Schmier, J.S. Klassen, Reliable determinations of protein–ligand interactions by direct ESI–MS measurements, are we there yet? *J. Am. Soc. Mass Spectrom.* 23 (2012) 431–441, <http://dx.doi.org/10.1007/s13361-011-0311-9>.
- [10] D. Cubrilovic, K. Barylyuk, D. Hofmann, M.J. Walczak, M. Gräber, T. Berg, et al., Direct monitoring of protein–protein inhibition using nano electrospray ionization mass spectrometry, *Chem. Sci.* 5 (2014) 2794, <http://dx.doi.org/10.1039/c3sc53360c>.
- [11] C.J. Hogan, E.M. Kettleson, B. Ramaswami, D.-R. Chen, P. Biswas, Charge reduced electrospray size spectrometry of mega- and gigadalton complexes: whole viruses and virus fragments, *Anal. Chem.* 78 (2006) 844–852, <http://dx.doi.org/10.1021/ac051571i>.
- [12] C.J. Hogan Jr., P. Biswas, Monte carlo simulation of macromolecular ionization by nanoelectrospray, *J. Am. Soc. Mass Spectrom.* 19 (2008) 1098–1107, <http://dx.doi.org/10.1016/j.jasms.2008.05.007>.
- [13] M. Li, S. Guha, R. Zangmeister, M.J. Tarlov, M.R. Zachariah, Quantification and compensation of nonspecific analyte aggregation in electrospray sampling, *Aerosol Sci. Technol.* 45 (2011) 849–860, <http://dx.doi.org/10.1080/02786826.2011.566901>.
- [14] M. Li, S. Guha, R. Zangmeister, M.J. Tarlov, M.R. Zachariah, Method for determining the absolute number concentration of nanoparticles from electrospray sources, *Langmuir* 27 (2011) 14732–14739, <http://dx.doi.org/10.1021/la202177s>.
- [15] A. Gomez, K. Tang, Charge and fission of droplets in electrostatic sprays, *Phys. Fluids* 6 (1994) 404–414, <http://dx.doi.org/10.1063/1.868037>.
- [16] Z. Olumee, J.H. Callahan, A. Vertes, Droplet dynamics changes in electrostatic sprays of methanol–water mixtures, *J. Phys. Chem. A* 102 (1998) 9154–9160, <http://dx.doi.org/10.1021/jp982027z>.
- [17] J.N. Smith, R.C. Flagan, J.L. Beauchamp, Droplet evaporation and discharge dynamics in electrospray ionization, *J. Phys. Chem. A* 106 (2002) 9957–9967, <http://dx.doi.org/10.1021/jp025723e>.
- [18] R. Juraschek, T. Dülcks, M. Karas, Nanoelectrospray—more than just a minimized-flow electrospray ionization source, *J. Am. Soc. Mass Spectrom.* 10 (1999) 300–308, [http://dx.doi.org/10.1016/S1044-0305\(98\)00157-3](http://dx.doi.org/10.1016/S1044-0305(98)00157-3).
- [19] A. Schmidt, M. Karas, T. Dülcks, Effect of different solution flow rates on analyte ion signals in nano-ESI MS, or: when does ESI turn into nano-ESI? *J. Am. Soc. Mass Spectrom.* 14 (2003) 492–500, [http://dx.doi.org/10.1016/S1044-0305\(03\)00128-4](http://dx.doi.org/10.1016/S1044-0305(03)00128-4).
- [20] X. Tang, J.E. Bruce, H.H. Hill, Characterizing electrospray ionization using atmospheric pressure ion mobility spectrometry, *Anal. Chem.* 78 (2006) 7751–7760, <http://dx.doi.org/10.1021/ac0613380>.
- [21] S. Ghosal, Mathematical modeling of electrokinetic effects in micro and nano fluids, in: S. Chakraborty (Ed.), *Microfluidics and Microfabrication*, Springer, US, 2010, pp. 87–112 (accessed 10.08.15) http://link.springer.com/chapter/10.1007/978-1-4419-1543-6_2.
- [22] M. Wilm, M. Mann, Analytical properties of the nanoelectrospray ion source, *Anal. Chem.* 68 (1996) 1–8, <http://dx.doi.org/10.1021/ac9509519>.
- [23] J.L.P. Benesch, B.T. Ruotolo, D.A. Simmons, C.V. Robinson, Protein complexes in the gas phase: technology for structural genomics and proteomics, *Chem. Rev.* 107 (2007) 3544–3567, <http://dx.doi.org/10.1021/cr068289b>.
- [24] B.M. Hossain, D.A. Simmons, L. Konermann, Do electrospray mass spectra reflect the ligand binding state of proteins in solution? *Can. J. Chem.* 83 (2005) 1953–1960, <http://dx.doi.org/10.1139/v05-194>.
- [25] J. Sun, E.N. Kitova, N. Sun, J.S. Klassen, Method: for identifying nonspecific protein–protein interactions in nanoelectrospray ionization mass spectrometry, *Anal. Chem.* 79 (2007) 8301–8311, <http://dx.doi.org/10.1021/ac0709347>.
- [26] N. Sun, J. Sun, E.N. Kitova, J.S. Klassen, Identifying nonspecific ligand binding in electrospray ionization mass spectrometry using the reporter molecule method, *J. Am. Soc. Mass Spectrom.* 20 (2009) 1242–1250, <http://dx.doi.org/10.1016/j.jasms.2009.02.024>.
- [27] L.A. Lane, B.T. Ruotolo, C.V. Robinson, G. Favrin, J.L.P. Benesch, A Monte Carlo approach for assessing the specificity of protein oligomers observed in nano-electrospray mass spectra, *Int. J. Mass Spectrom.* 283 (2009) 169–177, <http://dx.doi.org/10.1016/j.ijms.2009.03.006>.
- [28] K.C. Lewis, D.M. Dohmeier, J.W. Jorgenson, S.L. Kaufman, F. Zarrin, F.D. Dorman, Electrospray–condensation particle counter: a molecule–Counting LC detector for macromolecules, *Anal. Chem.* 66 (1994) 2285–2292, <http://dx.doi.org/10.1021/ac00086a014>.
- [29] C.J. Hogan, P. Biswas, Porous film deposition by electrohydrodynamic atomization of nanoparticle sols, *Aerosol Sci. Technol.* 42 (2008) 75–85, <http://dx.doi.org/10.1080/02786820701787951>.
- [30] A. Wortmann, A. Kistler-Momotova, R. Zenobi, M.C. Heine, O. Wilhelm, S.E. Pratsinis, Shrinking droplets in electrospray ionization and their influence on chemical equilibria, *J. Am. Soc. Mass Spectrom.* 18 (2007) 385–393, <http://dx.doi.org/10.1016/j.jasms.2006.10.010>.
- [31] S.L. Kaufman, J.W. Skogen, F.D. Dorman, F. Zarrin, K.C. Lewis, Macromolecule analysis based on electrophoretic mobility in air: globular proteins, *Anal. Chem.* 68 (1996) 1895–1904, <http://dx.doi.org/10.1021/ac951128f>.
- [32] G. Bacher, W.W. Szymanski, S.L. Kaufman, P. Zöllner, D. Blaas, G. Allmaier, Charge-reduced nano electrospray ionization combined with differential mobility analysis of peptides, proteins, glycoproteins, noncovalent protein complexes and viruses, *J. Mass Spectrom.* 36 (2001) 1038–1052, <http://dx.doi.org/10.1002/jms.208>.
- [33] J.F. de la Mora, S. Ude, B.A. Thomson, The potential of differential mobility analysis coupled to MS for the study of very large singly and multiply charged proteins and protein complexes in the gas phase, *Bioelectron. J.* 1 (2006) 988–997, <http://dx.doi.org/10.1002/biot.200600070>.
- [34] L.F. Pease, J.T. Elliott, D.-H. Tsai, M.R. Zachariah, M.J. Tarlov, Determination of protein aggregation with differential mobility analysis: application to IgG antibody, *Bioelectron. J.* 1 (2008) 1214–1222, <http://dx.doi.org/10.1002/biot.22017>.
- [35] J.Z. Bereszczak, M. Havlik, V.U. Weiss, M. Marchetti-Deschmann, E. van Duijn, N.R. Watts, et al., Sizing up large protein complexes by electrospray ionisation-based electrophoretic mobility and native mass spectrometry: morphology selective binding of Fabs to hepatitis B virus capsids, *Anal. Bioanal. Chem.* 406 (2014) 1437–1446, <http://dx.doi.org/10.1007/s00216-013-7548-z>.
- [36] A. Maißer, J.M. Thomas, C. Larriba-Andaluz, S. He, C.J. Hogan Jr., The mass–mobility distributions of ions produced by a Po-210 source in air, *J. Aerosol Sci.* 90 (2015) 36–50, <http://dx.doi.org/10.1016/j.jaerosci.2015.08.004>.

- [37] D.-R. Chen, D.Y.H. Pui, S.L. Kaufman, Electro-spraying of conducting liquids for monodisperse aerosol generation in the 4 nm–1.8 μm diameter range, *J. Aerosol Sci.* 26 (1995) 963–977, [http://dx.doi.org/10.1016/0021-8502\(95\)00027-A](http://dx.doi.org/10.1016/0021-8502(95)00027-A).
- [38] R. Gopalakrishnan, M.J. Meredith, C. Larriba-Andaluz, C.J. Hogan Jr., Brownian dynamics determination of the bipolar steady state charge distribution on spheres and non-spheres in the transition regime, *J. Aerosol Sci.* 63 (2013) 126–145, <http://dx.doi.org/10.1016/j.jaerosci.2013.04.007>.
- [39] D.-R. Chen, D.Y.H. Pui, D. Hummes, H. Fissan, F.R. Quant, G.J. Sem, Design and evaluation of a nanometer aerosol differential mobility analyzer (nano-DMA), *J. Aerosol Sci.* 29 (1998) 497–509, [http://dx.doi.org/10.1016/S0021-8502\(97\)10018-0](http://dx.doi.org/10.1016/S0021-8502(97)10018-0).
- [40] W. Liu, S.L. Kaufman, B.L. Osmondson, G.J. Sem, F.R. Quant, D.R. Oberreit, Water-based condensation particle counters for environmental monitoring of ultrafine particles, *J. Air Waste Manag. Assoc.* 56 (2006) 444–455.
- [41] S.C. Wang, R.C. Flagan, Scanning electrical mobility spectrometer, *Aerosol Sci. Technol.* 13 (1990) 230–240, <http://dx.doi.org/10.1080/02786829008959441>.
- [42] A. Wiedensohler, W. Birmili, A. Nowak, A. Sonntag, K. Weinhold, M. Merkel, et al., Mobility particle size spectrometers: harmonization of technical standards and data structure to facilitate high quality long-term observations of atmospheric particle number size distributions, *Atmos. Meas. Tech.* 5 (2012) 657–685, <http://dx.doi.org/10.5194/amt-5-657-2012>.
- [43] D.R. Oberreit, P.H. McMurry, C.J. Hogan, Mobility analysis of 2 nm–11 nm aerosol particles with an aspirating drift tube ion mobility spectrometer, *Aerosol Sci. Technol.* 48 (2014) 108–118, <http://dx.doi.org/10.1080/02786826.2013.861893>.
- [44] A.M. Gañán-Calvo, J. Dávila, A. Barrero, Current and droplet size in the electro-spraying of liquids. Scaling laws, *J. Aerosol Sci.* 28 (1997) 249–275, [http://dx.doi.org/10.1016/S0021-8502\(96\)00433-8](http://dx.doi.org/10.1016/S0021-8502(96)00433-8).
- [45] A. Srikanth, J. Karnawat, A. Kushari, The effect of charge density on electro-sprayed droplets, *Open Appl. Phys. J.* 2 (2009) 53–57.
- [46] M.S. Alexander, M.D. Paine, J.P.W. Stark, Pulsation modes and the effect of applied voltage on current and flow rate in nanoelectrospray, *Anal. Chem.* 78 (2006) 2658–2664, <http://dx.doi.org/10.1021/ac0520036>.
- [47] A. El-Faramawy, K.W.M. Siu, B.A. Thomson, Efficiency of nano-electrospray ionization, *J. Am. Soc. Mass Spectrom.* 16 (2005) 1702–1707, <http://dx.doi.org/10.1016/j.jasms.2005.06.011>.
- [48] M. Peschke, U.H. Verkerk, P. Kebarle, Features of the ESI mechanism that affect the observation of multiply charged noncovalent protein complexes and the determination of the association constant by the titration method, *J. Am. Soc. Mass Spectrom.* 15 (2004) 1424–1434, <http://dx.doi.org/10.1016/j.jasms.2004.05.005>.
- [49] *Handbook of Atomization and Sprays: Theory and Applications*, 2011 ed., Springer, New York, 2011.
- [50] R. Gopalakrishnan, C.J. Hogan, Coulomb-influenced collisions in aerosols and dusty plasmas, *Phys. Rev. E Stat. Nonlin. Soft Matter Phys.* 85 (2012) 026410, <http://dx.doi.org/10.1103/PhysRevE.85.026410>.
- [51] M.A. Abbas, J. Latham, The instability of evaporating charged drops, *J. Fluid Mech.* 30 (1967) 663–670, <http://dx.doi.org/10.1017/S0022112067001685>.
- [52] C.B. Richardson, A.L. Pigg, R.L. Hightower, On the stability limit of charged droplets, *Proc. R. Soc. Lond. A* 422 (1989) 319–328, <http://dx.doi.org/10.1098/rspa.1989.0031>.
- [53] D.C. Taffin, T.L. Ward, E.J. Davis, Electrified droplet fission and the Rayleigh limit, *Langmuir* 5 (1989) 376–384, <http://dx.doi.org/10.1021/la00086a016>.
- [54] E.J. Davis, M.A. Bridges, The rayleigh limit of charge revisited: light scattering from exploding droplets, *J. Aerosol Sci.* 25 (1994) 1179–1199, [http://dx.doi.org/10.1016/0021-8502\(94\)90208-9](http://dx.doi.org/10.1016/0021-8502(94)90208-9).